International Endodontic Journal

doi:10.1111/j.1365-2591.2011.01907.x

Fluoride-containing nanoporous calcium-silicate MTA cements for endodontics and oral surgery: early fluorapatite formation in a phosphate-containing solution

M. G. Gandolfi[1], P. Taddei[2], F. Siboni[1], E. Modena[2], M. P. Ginebra[3] & C. Prati[1]

[1]Laboratory of Biomaterials and Oral Pathology, Department of Odontostomatological Science, Endodontic, Clinical Section, University of Bologna, Bologna; [2]Department of Biochemistry, University of Bologna, Bologna, Italy; and [3]Division of Biomaterials, Bioceramics and Tissue Engineering, Department of Materials Science and Metallurgical Engineering, Technical University of Catalonia, Barcelona, Spain

Abstract

Gandolfi MG, Taddei P, Siboni F, Modena E, Ginebra MP, Prati C. Fluoride-containing nanoporous calcium-silicate MTA cements for endodontics and oral surgery: early fluorapatite formation in a phosphate-containing solution. *International Endodontic Journal*, **44**, 938–949, 2011.

Aim To test the chemical–physical properties and apatite-forming ability of experimental fluoride-doped calcium silicate cements designed to create novel bioactive materials for use in endodontics and oral surgery.

Methodology A thermally treated calcium silicate cement (wTC) containing $CaCl_2$ 5%wt was modified by adding NaF 1%wt (FTC) or 10%wt (F10TC). Cements were analysed by environmental scanning electron microscopy with energy-dispersive X-ray analysis, IR and micro-Raman spectroscopy in wet conditions immediately after preparation or after ageing in a phosphate-containing solution (Dulbecco's phosphate-buffered saline). Calcium and fluoride release and pH of the storage solution were measured. The results obtained were analysed statistically (Tukey's HSD test and two-way ANOVA).

Results The formation of calcium phosphate precipitates (spherulites) was observed on the surface of 24 h-aged cements and the formation of a thick bone-like B-type carbonated apatite layer (biocoating) on 28 day-aged cements. The rate of apatite formation was FTC > F10TC > wTC. Fluorapatite was detected on FTC and F10TC after 1 day of ageing, with a higher fluoride content on F10TC. All the cements released calcium ions. At 5 and 24 h, the wTC had the significantly highest calcium release ($P < 0.001$) that decreased significantly over the storage time. At 3–28 days, FTC and F10TC had significantly higher calcium release than wTC ($P < 0.05$). The F10TC had the significantly highest fluoride release at all times ($P < 0.01$) that decreased significantly over storage time. No significant differences were observed between FTC and wTC. All the cements had a strong alkalinizing activity (OH^- release) that remained after 28 days of storage.

Conclusions The addition of sodium fluoride accelerated apatite formation on calcium silicate cements. Fluoride-doped calcium silicate cements had higher bioactivity and earlier formation of fluorapatite. Sodium fluoride may be introduced in the formulation of mineral trioxide aggregate cements to enhance their biological behaviour. F-doped calcium silicate cements are promising bone cements for clinical endodontic use.

Keywords: apatite, bioactive materials, calcium hydroxide, calcium release, calcium-silicate cements, endodontic cements, fluorapatite, fluoride release, fluoride-doped MTA, mineral trioxide aggregate.

Received 1 February 2011; accepted 14 May 2011

Correspondence: Maria Giovanna Gandolfi, DBiol, DSc, MBiol, PhD, Head Laboratory of Biomaterials and Oral Pathology, Department of Odontostomatological Sciences, University of Bologna, Via San Vitale 59, 40125 Bologna, Italy (e-mail: mgiovanna.gandolfi@unibo.it).

Introduction

Calcium silicate cements, well known as mineral trioxide aggregate (MTA), are novel self-setting biomaterials for oral and endodontic surgery (Parirokh & Torabinejad 2010). The setting reaction of calcium silicate cements requires water, so that they are able to set in a wet environment through the formation of a nanoporous calcium silicate hydrate (CSH) gel.

Calcium silicate MTA cements are biointeractive bioactive materials, i.e. materials able to exchange information with a biological system (this encompasses a physicochemical interplay between the material surface and the biological environment) (biointeractivity) and materials able to evoke a positive response from the host body (bioactivity) (BSI, 2007). A number of investigations have demonstrated that when calcium silicate MTA cements are exposed to simulated extracellular fluids containing a phosphate source, they form calcium phosphates and apatite precipitates on their surface (Gandolfi *et al.* 2009a, 2010a-d, Taddei *et al.* 2009a, 2009b, Torrisi *et al.* 2010; Taddei *et al.* 2011). Calcium ions released from MTA react with phosphates provided by the simulated fluid causing apatite formation. The sealing ability, biocompatibility and dentinogenic activity of MTA cements may be improved and favoured by their bioactivity properties and the formation of apatite.

Fluoride-doped calcium silicate MTA cements have recently been designed and studied (Gandolfi *et al.* 2009b, Gandolfi & Prati 2010e, Colin *et al.* 2010). It has been reported that (i) the addition of sodium fluoride 1%wt to calcium silicate powders causes a delay in the setting time and increases expansion (Gandolfi *et al.* 2009b) and long-term apical sealing ability in the root canal (Gandolfi & Prati 2010e) and (ii) an increase in NaF content (from 0% to 10%wt) results in an enhanced solubility of F-doped MTA cements in water or in Dulbecco's modified eagle medium (DMEM) (Colin *et al.* 2010).

This study aimed to evaluate the effect of the sodium fluoride content in experimental MTA cements on the kinetics of apatite formation and ion release. The bioactivity of experimental fluoride-doped calcium silicate cements was investigated by environmental scanning electron microscopy coupled with energy-dispersive X-ray analysis (ESEM-EDX), micro-Raman and Fourier transform infrared spectroscopy (FTIR) analyses, after storage in a simulated extracellular fluid solution.

Materials and methods

Cement preparation

The experimental thermally treated calcium silicate cement (identified as wTC) composed of di- and tricalcium silicate, tricalcium aluminate, calcium sulphate, calcium chloride (setting accelerator) and bismuth oxide (radiopacifying agent) was prepared (Gandolfi *et al.* 2010d). Sodium fluoride 1% wt or 10% wt was added to wTC to produce two experimental fluoride-doped cements, identified as FTC and F10TC, respectively (Gandolfi, Laboratory of Biomaterials, University of Bologna, Bologna, Italy).

The cements were mixed with Dulbecco's phosphate-buffered saline (Dulbecco's phosphate-buffered saline (DPBS), cat. n.BE17-512; Lonza, Verviers, Belgium) as a source of phosphate ions, using a liquid/powder ratio of 0.3 to produce a homogeneous paste. After preparation, the cement pastes were placed in PVC moulds (8 mm diameter and 1.6 mm thick) to prepare standard discs.

In vitro apatite-forming ability (bioactivity)

The ability of the different materials to form apatite on their surface was tested *in vitro* as an index of bioactivity (BSI, 2007, Kokubo & Takadama 2006). Bioactivity tests were carried out in DPBS (Gandolfi *et al.* 2010a-d, Taddei *et al.* 2009a, 2009b, Taddei *et al.* 2010). DPBS is a physiological-like buffered (pH 7.4) Ca- and Mg-free solution with the following composition (mmol L^{-1}): K^+ (4.18), Na^+ (152.9), Cl^- (139.5) and PO_4^{3-} (9.56, sum of $H_2PO_4^-$ 1.5 mmol L^{-1} and HPO_4^{2-} 8.06 mmol L^{-1}).

Each cement disc was placed in a hermetically sealed cylindrical polystyrene container (3 cm high and 4 cm in diameter) containing 5 mL DPBS (15 mL of medium for 1 g of cement paste) and was maintained at 37 °C until the pre-determined end-point time (1, 7 and 28 days).

The phosphate ions (as $H_2PO_4^-$ and HPO_4^{2-}) were continuously supplied by the DPBS solution that was renewed after 5 and 24 h and 7, 14 and 28 days.

The cements were analysed by ESEM/EDX, micro-Raman and FTIR spectroscopy immediately after preparation (fresh unset samples 10 min old) and after 1 and 28 days of ageing in DPBS (1 day-aged group and 28 day-aged group). The constituent cement powders (anhydrous powders) were also analysed.

Environmental scanning electron microscopy with energy-dispersive X-ray analysis

Samples were examined under an environmental scanning electron microscope (ESEM Zeiss EVO 50; Carl Zeiss, Oberkochen, Germany) connected to a secondary electron detector for energy-dispersive X-ray analysis EDX (INCA 350 EDS, Oxford Instruments, Abingdon, UK) computer controlled software INCA energy version 18 (Oxford Instruments, Abingdon, UK), using an accelerating voltage of 20–25 kV. The elemental analysis (weight % and atomic %) of samples was carried out applying the ZAF correction method. At 25 kV acceleration, the X-ray electron beam penetration of ESEM-EDX (inside a material with a density of about 3 g cm^{-3}) proved to be 2.98 μm and consequently the volume excited and involved in the emission of characteristic X-rays from the constituting elements was considered to be 10 μm^3. Cement discs were placed directly on the ESEM stub and examined without preparation (samples were not coated for this analysis).

Micro-Raman and ATR/FTIR spectroscopy

Micro-Raman spectra were obtained using a Jasco NRS-2000C instrument (Jasco Inc., Easton, MD, USA) connected to a microscope with 20× magnification. In these conditions, the laser spot size (i.e. the excitation source) was of the order of a few microns. All the spectra were recorded in back-scattering conditions with 5 cm^{-1} spectral resolutions using the 488-nm line (Innova Coherent 70; Coherent Inc., Santa Clara, CA, USA)) with a power of 50 mW. A 160 K frozen Charge Coupled Device detector from Princeton Instruments Inc (Trenton, NJ, USA) was used.

IR spectra were recorded on a Nicolet 5700 FTIR spectrometer (Thermo Electron Scientific Instruments Corp., Madison, WI, USA) equipped with a Smart Orbit diamond attenuated total reflectance (ATR) accessory and a Deuterated Tri-Glycine Sulphate detector; the spectral resolution was 4 cm^{-1}, and 64 scans were made for each spectrum. The ATR area had a 2 mm diameter. The IR radiation penetration was about two microns.

To minimize the variability deriving from possible sample inhomogeneity, at least five spectra were recorded on five different points on the upper surface of each specimen. The Raman spectra were recorded on wet cement samples (i.e. when maintained in their storage media).

pH of storage solution and calcium and fluoride release

Each cement disc was placed in a hermetically sealed cylindrical polystyrene holder (3 cm high, 4 cm diameter) containing 10 mL water and was maintained at 37 °C until the pre-determined end-point time (5 h, 24 h, 3, 7, 14 and 28 days). At each end-point time, the storage water was analysed for pH as well as calcium and fluoride content and renewed. The pH was measured using a (selective) temperature-compensated electrode (Sen Tix Sur WTW, Weilheim, Germany) connected to a multiparameter laboratory meter (inoLab 750; WTW).

For calcium quantization, 0.100 mL (2%) of ISA (4 mol L^{-1} KCl; WTW) was added to 5 mL of storage medium, and the calcium content was evaluated using a calcium probe (Calcium ion electrode; Eutech instruments Pte Ldt, Singapore) connected to a multiparameter laboratory meter (inoLab 750; WTW).

For fluoride assessment, 5 mL of TISAB (sodium chloride 5.8% w/v, acetic acid 5.7% w/v, sodium hydroxide 3.0% (w/v), CDTA 0.4% (w/v) and water; WTW) was added to 5 mL of storage solution, and the fluoride content was evaluated using a fluoride probe (Fluoride ion electrode; Eutech instruments Pte Ldt) connected to a multiparameter laboratory meter (inoLab 750; WTW). The probes were inserted in the storage media at room temperature (24 °C) under magnetic stirring. Each measurement was repeated three times.

The results obtained were analysed statistically. Tukey's HSD (honestly significant differences) test was used in conjunction with the two-way analysis of variance (two-way ANOVA), to determine the statistical significance of the differences among the groups.

Results

Environmental scanning electron microscopy with energy-dispersive X-ray analysis

Starting cement powders (unhydrated cement powders) (Figs 1a, 2a and 3a) showed the reflexes of Ca (calcium), Si (silicon) and Al (aluminium) from the cement particles, Bi (bismuth) from the Bi_2O_3 radiopacifier, Cl (chlorine) from the $CaCl_2$ setting accelerator, O (oxygen) from the cement particles and the radiopacifier. In addition, the F-doped powders showed Na (sodium) and F (fluorine) from sodium fluoride.

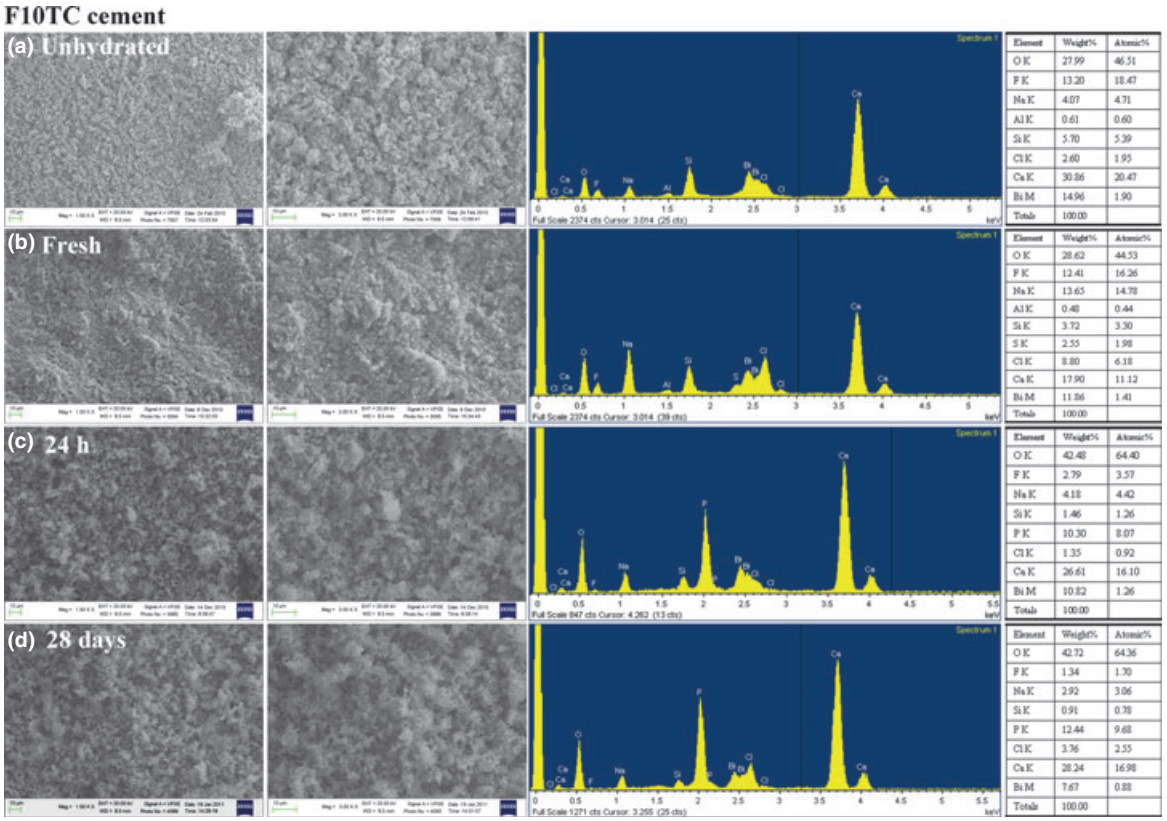

Element	Weight%	Atomic%
O K	27.99	46.51
F K	13.20	18.47
Na K	4.07	4.71
Al K	0.61	0.60
Si K	5.70	5.39
Cl K	2.60	1.95
Ca K	30.86	20.47
Bi M	14.96	1.90
Totals	100.00	

Element	Weight%	Atomic%
O K	28.62	44.53
F K	12.41	16.26
Na K	13.65	14.78
Al K	0.48	0.44
Si K	3.72	3.30
S K	2.55	1.98
Cl K	8.80	6.18
Ca K	17.90	11.12
Bi M	11.86	1.41
Totals	100.00	

Element	Weight%	Atomic%
O K	42.48	64.40
F K	2.79	3.57
Na K	4.18	4.42
Si K	1.46	1.26
P K	10.30	8.07
Cl K	1.35	0.92
Ca K	26.61	16.10
Bi M	10.82	1.26
Totals	100.00	

Element	Weight%	Atomic%
O K	42.72	64.36
F K	1.34	1.70
Na K	2.92	3.06
Si K	0.91	0.78
P K	12.44	9.68
Cl K	3.76	2.55
Ca K	28.24	16.98
Bi M	7.67	0.88
Totals	100.00	

Figure 1 F10TC cement: environmental scanning electron microscopy with energy-dispersive X-ray analyses of unhydrated powder (a), freshly prepared (b), 24 h-aged (c) and 28 day-aged (d) samples.

The surface of fresh cements (Figs 1b, 2b and 3b) appeared rough/irregular and free from porosities. EDX showed prominent peaks because of Ca, Cl and O (from the cement particles, the radiopacifier and water), S (sulphur), Si (also from the silanol groups of CSH) and Bi.

The surface of 24 h-aged samples (Figs 1c, 2c and 3c) showed diffuse deposits with different size and shape, composed of globular precipitates (spherulites, 0.2–1 micron diameter). The deposit was more evident and thicker on F-containing cements (Figs 1c and 2c).

Energy-dispersive X-ray analysis microanalysis on the area (approximately 3000 μ^2) displayed prominent Ca, P (phosphorous) and O reflexes and traces of Si, Bi and Cl components. The intensity of the typical elements of the cement (mainly silicon) decreased over storage time because of the formation of the calcium phosphate layer (biocoating).

FTC and F10TC samples displayed higher P peaks and lower Ca/P ratio approximately 2.2–2.5) than wTC (approximately 3.2): the Ca peak detected on the wTC cement originated from the calcium phosphate deposits, the calcium silicate component and the $CaCl_2$ ingredient.

Punctual EDX on spherulites showed only Ca and P peaks, suggesting the formation of calcium phosphate precipitates.

Environmental scanning electron microscopy observations of the surface of 28 day-aged samples (Figs 1d, 2d and 3d) showed a continuous irregular layer of deposits. No morphological differences were noted among the cements.

Energy-dispersive X-ray analysis detected prevalent Ca and P peaks and traces of typical elements of the cement, suggesting the formation of a thick calcium phosphate layer that is able to mask the underlying components of the cement. FTC and F10TC samples displayed lower Ca/P ratio than wTC.

Punctual EDX registered Ca and P with a Ca/P ratio (approximately 2) close to that of bone-like carbonated apatites.

The Ca/P ratio on the calcium phosphate layer decreased during immersion in DPBS (from

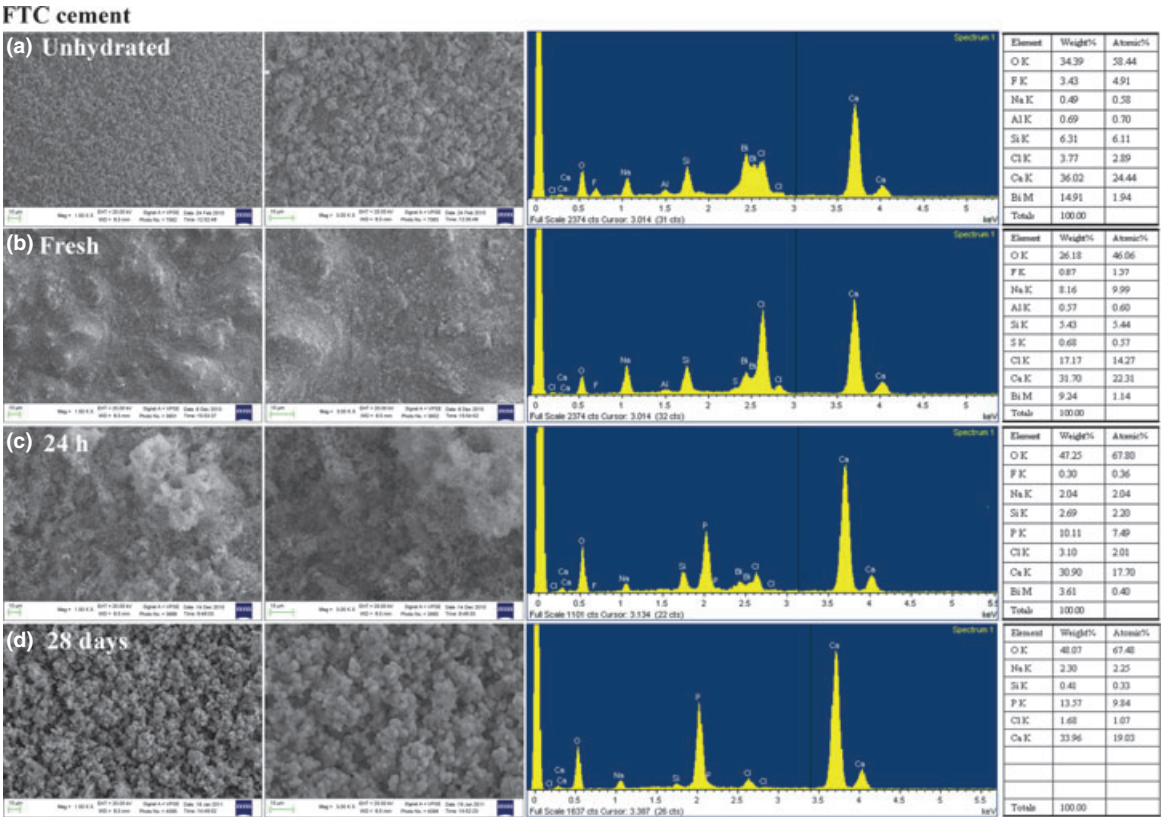

Figure 2 FTC cement: environmental scanning electron microscopy with energy-dispersive X-ray analyses of unhydrated powder (a), freshly prepared (b), 24 h-aged (c) and 28 day-aged (d) samples.

approximately 2.5–3.0 at 24 h to approximately 2 at 28 days) for all the cements. The presence of $CaCl_2$ may have slightly affected the Ca/P ratio detected on the samples covered by a calcium phosphate layer thinner than the X-ray electron beam penetration, i.e. approximately 2.98 μm. The contribution of $CaCl_2$ to the observed Ca/P ratio decreased at increasing deposit thickness, i.e. at increasing ageing time.

Micro-Raman analyses

Figure 4 reports the micro-Raman spectra recorded on the cements. Bands were assigned according to the literature (Taddei *et al.* 2009a,b, 2011 and references cited therein).

The spectra of the unhydrated powders practically coincided and disclosed calcium carbonate (band at 1087–1088 cm^{-1}), calcium sulphate as both anhydrite (band at 1017 cm^{-1}) and gypsum (band at 1002–1003 cm^{-1}), alite (band at 845 cm^{-1}), belite (bands at 855 and 845 cm^{-1}) and bismuth oxide (bands below 600 cm^{-1}).

The freshly prepared samples revealed the appearance of the marker band of ettringite (i.e. the hydration product of the reaction between anhydrite/gypsum and tricalcium aluminate) at about 990 cm^{-1}, particularly strong on the F10TC cement.

After 1 day of ageing in DPBS, all the cements showed an apatite + calcite/aragonite deposit. Apatite was revealed by the appearance of the band at 960 cm^{-1}, and the bands at 1000, 1045 and 1070 cm^{-1} (typical of a B-type carbonated apatite) and 607 and 590 cm^{-1} (FTC) were also detected on the F-doped cements. The intensity ratio between the bands of apatite and belite (at about 960 and 855 cm^{-1}, respectively) was taken as a marker of the thickness of the apatite deposit. This ratio was higher on the F-doped cements than on wTC. The 960 cm^{-1} apatite band was broader on F10TC than on FTC, and an analogous trend was observed after 7 days of ageing.

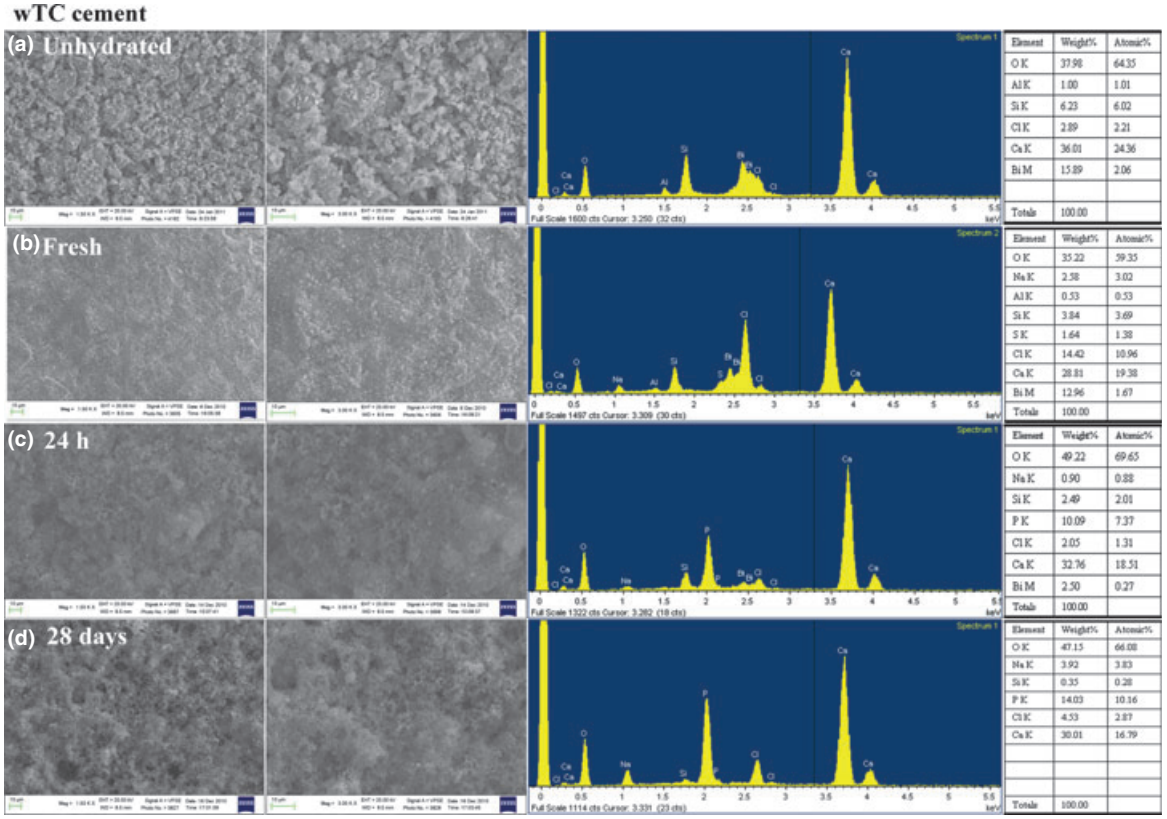

Figure 3 wTC cement: environmental scanning electron microscopy with energy-dispersive X-ray analyses of unhydrated powder (a), freshly prepared (b), 24 h-aged (c) and 28 day-aged samples (d).

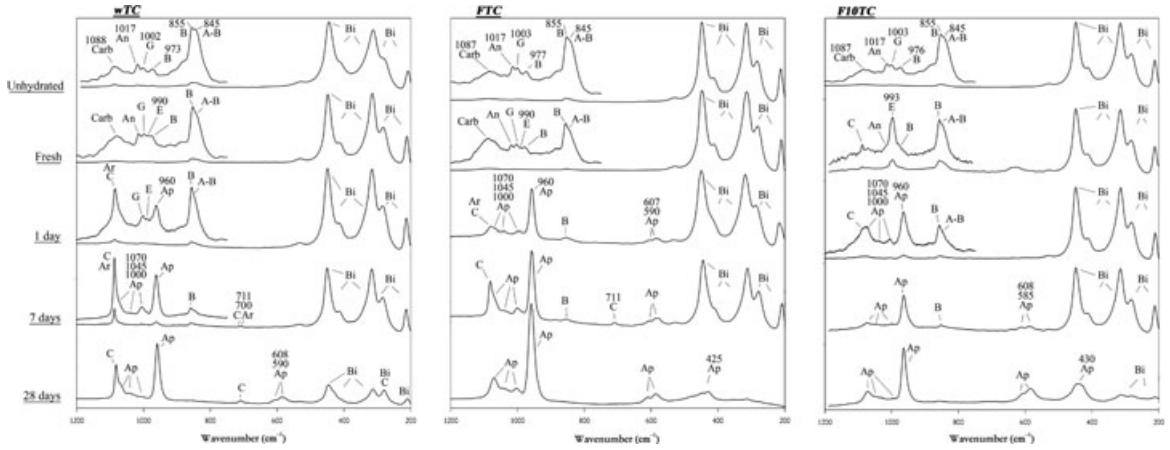

Figure 4 Micro-Raman spectra recorded on the surface of the three cements: freshly prepared (after 10 min) and after 1 and 28 days of ageing in Dulbecco's phosphate-buffered saline. The bands owing to calcium carbonate (Carb), calcite (C), aragonite (Ar), anhydrite (An), gypsum (G), ettringite (E), belite (B), alite (A), apatite (Ap) and bismuth oxide (Bi) are indicated. The spectra of the unhydrated cement powders are reported for comparison.

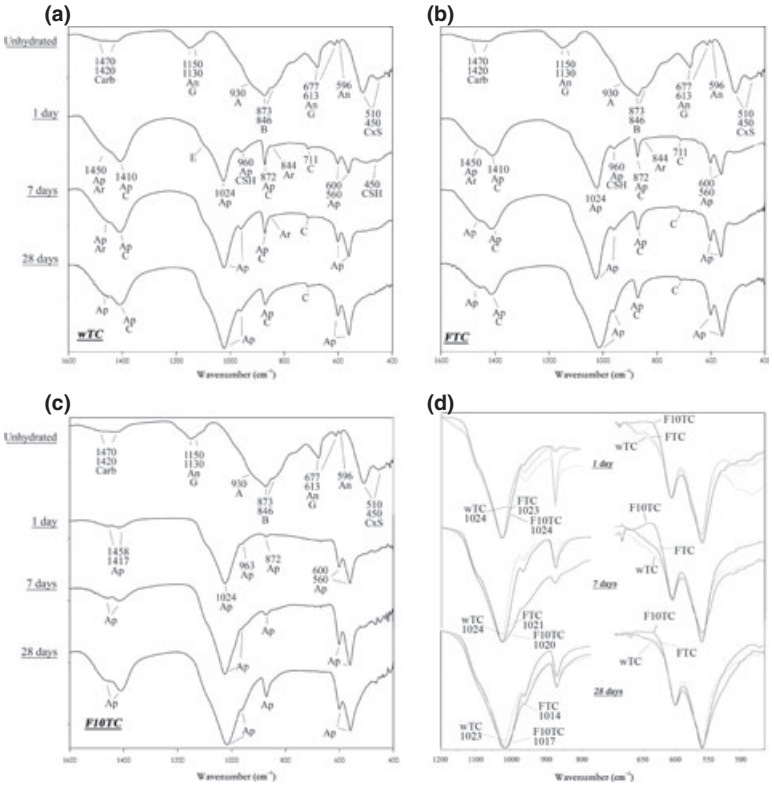

Figure 5 (a–c) IR spectra recorded on the surface of the three cements after 1 and 28 days of ageing in Dulbecco's phosphate-buffered saline (DPBS). The bands owing to calcium carbonate (Carb), calcite (C), aragonite (Ar), anhydrite (An), gypsum (G), ettringite (E), hydrated calcium silicate gel, slightly polymerized silicates (CxS), belite (B), alite (A) and apatite (Ap) are indicated. The spectra of the unhydrated cement powders are reported for comparison. (D) IR spectra recorded on the powders isolated from the DPBS storage media after 1, 7 and 28 days of ageing.

At increasing storage times, the bands of the cement progressively weakened, while the bands typical of a B-type carbonated apatite progressively strengthened. After 7 days of ageing in DPBS, the intensity ratio between the bands of apatite and belite had decreased along the series: FTC > F10TC > wTC. An analogous result was obtained after 28 days of ageing: the bands of bismuth oxide were observed with a progressively increasing intensity going from FTC to F10TC and wTC.

ATR/FTIR analyses

Figure 5 reports the IR spectra recorded on the cements. Bands were assigned according to the literature (Taddei *et al.* 2009a, 2011 and references cited therein).

The IR spectra of the unhydrated cements coincided and confirmed the presence of calcium carbonate (bands at 1420 and 1470 cm^{-1}), anhydrite (bands at 1150, 1130, 677, 613 and 596 cm^{-1}), gypsum (bands at 1150, 1130, 677 and 613 cm^{-1}) and slightly polymerized silicate groups (bands at 510 and 450 cm^{-1}) in the alite (marker band at 930 cm^{-1}) and belite (marker bands at 873 and 846 cm^{-1}) forms.

After 1 day of ageing in DPBS, all the cements had a B-type carbonated apatite deposit varying in thickness on the different samples, according to the Raman results. The spectra recorded on the surface of FTC and F10TC surfaces did not show any band of the underlying cement, and the deposit was mainly constituted by B-type carbonated apatite (bands at about 1450, 1410, 1024, 960, 872, 600 and 560 cm^{-1}) and calcite/aragonite indicating that the deposit was thicker than 2 μm.

The apatite bands on F10TC were broader than on FTC (in particular those at 1024 and 963 cm^{-1}), according to the Raman findings. Besides B-type carbonated apatite and calcite/aragonite, the spectrum recorded on the surface of wTC showed the components

owing to the hydration of the cement (CSH and ettringite), suggesting that the deposit was thinner than 2 μm (i.e. thinner than on the F-doped cements).

After 7 days of ageing, the cement components also became undetectable on wTC, owing to the increased thickness of the deposit. After 7 and 28 days, the apatite bands on F10TC were also broader than on FTC. The same trend was observed in the spectra recorded on the powders isolated from the ageing media (Fig. 5d). These spectra showed a different trend for the different cements also in the range near 630 cm^{-1}, where the OH bending mode falls. At all the ageing times, the prominent feature observed for wTC progressively weakened going to FTC and F10TC. According to a previous study (Amberg *et al.* 1974), this trend suggests that the apatite deposit on FTC and F10TC contained increasing amounts of fluoride in the lattice.

pH of storage water and calcium and fluoride release

The pH of storage water after immersion of the cements is reported in Table 1a. All the cements had a strong alkalinizing activity (ability to release hydroxyl ions): the pH of the deionized storage water (approximately pH 6.8) increased significantly up to pH 12 during the first 5 h of immersion and decreased significantly over time.

NaF-doped cements caused a statistically higher increase of the pH at all end-points, and the pH rise (alkalinizing activity) of F10TC was stronger than FTC. The addition of fluoride increased the pH mainly at short storage times.

The alkalinizing activity of all the cements remained after 28 days of storage.

The calcium release of cements when soaked in deionized water is shown in Table 1b. All the cements released calcium ions. The calcium release from wTC decreased statistically over the storage time. At 5 and 24 h, the wTC had the significantly highest calcium release ($P < 0.001$), but at 3–28 days, FTC and F10TC had significantly higher calcium release than wTC ($P < 0.05$).

The fluoride release of cements when soaked in deionized water is shown in Table 1c. The F10TC showed the statistically highest fluoride release at all times ($P < 0.01$). The fluoride release statistically decreased over time. No significant differences were proved between FTC and wTC.

Discussion

Bioactive calcium silicate cements precipitate hydroxy-carbonated apatite onto their surface (Gandolfi *et al.* 2010a-c, Taddei *et al.* 2009a, 2009b) on dentine and inside the dentinal tubules (Gandolfi *et al.* 2008a).

It has been demonstrated that silanol groups form from hydrated calcium silicate upon cement powder hydration (after mixing with water). Phosphate ions from DPBS are absorbed by the silanol groups allowing the formation/nucleation of small round-shaped calcium phosphate precipitates named apatite spherulites (Gandolfi *et al.* 2010c).

Calcium silicate MTA cements for endodontic surgery (root-end filling materials and endodontic sealers) are used directly in contact with alveolar bone: a

Table 1 (a) pH of soaking water, (b) calcium and (c) fluoride released (ppm) in soaking water. Samples disks ($n = 10$ for each material) were used. The data (expressed as mean and standard deviation) were statistically analyzed using one-way ANOVA with Tukey test ($P < 0.05$). Different *CAPITAL* superscript letters in the same row or different *small* superscript letters in the same column mean statistically significant differences.

Material	5 h	1 day	3 days	7 days	14 days	28 days
(a)						
F10TC	12.49 ± 0.04^{A,a}	11.80 ± 0.10^{B,a}	9.74 ± 0.22^{C,a}	9.63 ± 0.42^{C,a}	8.81 ± 0.50^{D,a}	8.93 ± 0.34^{D,a}
FTC	11.82 ± 0.08^{A,b}	11.24 ± 0.16^{B,b}	10.37 ± 0.31^{c,b}	8.96 ± 0.16^{D,b}	8.95 ± 0.07^{D,ab}	8.84 ± 0.12^{D,a}
wTC	11.73 ± 0.11^{A,b}	11.23 ± 0.12^{B,b}	9.52 ± 0.26^{c,a}	9.26 ± 0.06^{CD,c}	9.05 ± 0.21^{D,b}	8.50 ± 0.11^{E,b}
(b)						
F10TC	21.13 ± 4.40^{A,a}	6.57 ± 4.70^{B,a}	35.80 ± 5.47^{C,a}	23.10 ± 2.25^{A,a}	11.23 ± 0.93^{B,a}	24.35 ± 1.52^{A,a}
FTC	21.88 ± 7.65^{A,a}	8.12 ± 1.45^{B,a}	32.30 ± 0.94^{C,a}	29.77 ± 1.19^{C,b}	19.71 ± 1.63^{A,b}	18.40 ± 1.06^{A,a}
wTC	440.22 ± 17.10^{A,b}	193.92 ± 16.95^{B,b}	25.21 ± 0.96^{C,b}	11.56 ± 1.40^{D,c}	10.14 ± 3.04^{D,a}	12.89 ± 1.72^{D,b}
(c)						
F10TC	9.33 ± 3.13^{A,a}	3.78 ± 0.66^{B,a}	1.89 ± 0.24^{C,a}	1.71 ± 0.25^{C,a}	1.51 ± 0.16^{C,a}	2.35 ± 0.35^{C,a}
FTC	1.24 ± 0.19^{A,b}	0.50 ± 0.08^{B,b}	0.35 ± 0.03^{B,b}	0.58 ± 0.10^{B,b}	0.58 ±0.07^{B,b}	0.52 ± 0.08^{B,b}
wTC	0.48 ± 0.19^{A,b}	0.37 ± 0.4^{A,b}	0.22 ± 0.02^{A,b}	0.26 ± 0.03^{A,b}	0.27 ± 0.08^{A,b}	0.25 ± 0.04^{A,b}

root-end filling material is positioned in the root-end cavity to seal the resected apex, and an endodontic sealer is frequently extruded from the apex in clinical practice. Therefore, osteoconductive activity is an essential property to support an adequate biological response and new bone tissue formation.

It is well known that sodium fluoride possesses good biological activity on bone/osteoblast cells and dental pulp cells (Lau & Baylink 1998, Nakade *et al.* 1999, Abdullah *et al.* 2002) and may be introduced in the formulation of MTA cements to improve their biological behaviour (Gandolfi *et al.* 2008b). Moreover, fluorapatite $Ca_{10}(PO_4)_6OH\text{-}F$ is more active on osteoblast activity and bone formation than hydroxyapatite $Ca_5(PO_4)_3OH$ (Qu & Wei 2006). The introduction of fluoride into apatite has been shown to improve osteoblast response in terms of adhesion (Qu & Wei 2006), differentiation (Qu & Wei 2006), proliferation (Yoon *et al.* 2005, Qu *et al.* 2008) and mineralization processes (Zhang *et al.* 1998) when compared to pure hydroxyapatite. The incorporation of fluorapatite into implant coatings improves implant integration into bone (Bhadang *et al.* 2010).

Sodium fluoride has been added to bone cements to speed up the early formation of bone at the interface and thereby improve fixation (Sundfeldt *et al.* 2002, Cartmell 2009). A recent study (Lin *et al.* 2009) investigated the effects of CaF_2 (0, 1, 2 and 3 wt%) on the apatite formation ability of tricalcium silicates (Ca_3SiO_5) and the mechanism of apatite formation in simulated body fluid. CaF_2-doped tricalcium silicates showed a better bioactivity than Ca_3SiO_5 owing to the formation and stability of F-substituted apatite (Lin *et al.* 2009). Fluoride-containing tricalcium silicates (Xu *et al.* 2008, Lin *et al.* 2009) or bioactive glasses (Brauer *et al.* 2008, 2010)) doped with CaF_2 have been studied for their ability to form F-substituted apatite. However, CaF_2 has a only limited solubility (K_{sp} 3.9×10^{-11}), which decreases in an alkaline environment. Therefore, NaF was selected in the present study for its greater solubility.

The results demonstrated that the NaF-doped calcium silicate cements were able to increase strongly the pH of storage water up to pH 12 during the first day of immersion. The addition of fluoride enhanced this pH rise mainly for short storage times. This result showed that NaF has a significantly different (i.e. opposite) effect from that exerted by CaF_2 (Lin *et al.* 2009), which has been reported to decrease cement hydration resulting in a lower alkalinizing activity (i.e. lower pH values).

F-containing cements released significantly lower amounts of calcium ions into the storage water than wTC (Table 1b). This result was not surprising because the F-containing cements allow the precipitation of calcium fluoride (fluorite) because of the presence of F^- ions. This phase was detected (data not shown) on the surface of the F-doped cements aged in water.

Raman and IR spectroscopies have been used to investigate the thickness of the deposit as well as its chemical nature. Both techniques revealed that in DPBS, FTC and F10TC had a more pronounced apatite-forming ability than wTC. Because of its low sampling depth, ATR/FTIR spectroscopy was able to yield information on the relative thickness of the deposits only at 1 day of ageing when the bands of the underlying cement were observed only for wTC. This behaviour suggested that the deposit was thinner on wTC than on the F-doped cements. Because of its higher sampling depth, Raman spectroscopy was able to discriminate among the three cements at all ageing times. The intensity ratio between the bands of apatite and belite differed significantly among the three cements and showed that bioactivity decreased along the series: FTC > F10TC > wTC.

Vibrational Raman and IR spectroscopy also yielded information on the chemical composition of the deposits. Both techniques showed that for all the cements, the apatite lattice contained carbonate in B-site (i.e. carbonate substitutes the phosphate ion in the lattice), as revealed by the marker bands of B-type carbonated apatites at about 1070 cm^{-1} (Raman), 1450–1410 and 870 cm^{-1} (IR). The broadening of the phosphate bands observed for F10TC in both the Raman and IR spectra suggested that on this cement, the apatite deposit was less crystalline than on the other cements. IR spectroscopy appeared more sensitive than Raman spectroscopy in the analysis of the fluoridation degree of the apatite formed on F-doped cements. It is well known that the fluoridation mechanism involves a hydroxyl substitution and a subsequent adjacent hydroxyl rearrangement. As a consequence, the intensity of the OH bending mode at about 630 cm^{-1} has been reported to decrease as the extent of fluoridation increases (Amberg *et al.* 1974). As shown in Fig. 5d, at all ageing times, the spectral feature at about 630 cm^{-1} appeared with decreasing intensity along the series wTC > FTC > F10TC. On this basis, it can be affirmed that the cements under study formed different apatite phases upon ageing in DPBS: a hydroxy-carbonated apatite formed on the surface of wTC, while from 1 day of ageing, the apatite

phase on FTC and F10TC contained increasing amounts of fluoride ions in the lattice. The incorporation of fluoride ions into the lattice can explain the higher bioactivity of the F-doped cements in DPBS, because F-substituted apatites have a lower K_{sp} than hydroxy-carbonate apatite.

The trend of the micro-Raman spectra suggested that FTC should have a higher bioactivity than F10TC. In other words, the increase in the fluoride content up to 10%wt did not lead to an improvement in the apatite-forming ability. This finding was not surprising in the light of a previous study (Lin *et al.* 2009) who reported that among the tricalcium silicate samples doped with 1, 2 and 3 wt% of CaF_2, the specimen with the intermediate fluoride content (i.e. 2%wt) had the highest bioactivity.

The mechanism of apatite formation on NaF-doped calcium silicate MTA cements may be proposed in the following stages:

- Stage I: when the calcium silicate powder reacts with water, CSH gel and $Ca(OH)_2$ are the main products; $Ca(OH)_2$ was detected in the IR spectra recorded in the interior of the cement discs (not shown). As Ca^{2+} and OH^- were rapidly released into the storage solution, the pH values increased. In addition, NaF-doped cement pastes can release F^- (Table 1c).
- Stage II: before the apatite formation, the surface layer of CSH gel formed in the calcium silicate pastes mainly consists of silanol groups $Si(OH)_4$, whose presence can be inferred from the IR band at 960 cm^{-1} (Lin *et al.* 2009). This band was observed in the IR spectra recorded in the interior of the cement discs (not shown).
- Stage III: the CSH gel layer provides the negatively charged sites for the migration of Ca^{2+} and PO_4^{3-} ions to the paste surface, followed by growth of an F-substituted apatite (Fig. 5d) layer by the incorporation of soluble F^- because F-substituted apatite has a lower K_{sp} (6.5×10^{-65}) than that of hydroxy-apatite $Ca_5(PO_4)_3OH$ ($K_{sp} = 7.36 \times 10^{-60}$).
- Stage IV: the F-substituted apatite acts as a new nucleation centre promoting the crystallization of the $CaO\text{-}P_2O_5$ layer by the incorporation of Ca^{2+}, PO_4^{3-}, CO_3^{2-} and F^- to form an apatite layer.

The study demonstrated that fluoride-doped calcium silicate cements are biointeractive materials able to release calcium and hydroxyl ions and form fluorapatite on their surface.

The calcium released by these cements affects osteoblast viability, proliferation and differentiation (Maeno *et al.* 2005, Sun *et al.* 2009a,b) and may have several biologically important functions in many clinical applications such as pulp capping procedures (Nair *et al.* 2008, Tuna & Ölmez 2008) and apexogenesis (Holden *et al.* 2008). Apatite formation represents a biological substrate for all clinical applications in bone tissue and may have a clinical effect on damaged tissues where new bone formation is required (Nair 2006). These data may explain the positive reports on the use of calcium silicate cements such as ProRoot MTA, MTA Angelus and Tech Biosealer in clinical situations (Saunders 2008, Pace *et al.* 2008, Parirokh & Torabinejad 2010).

Conclusions

Fluoride-doped calcium silicate cements form fluorapatite in phosphate-containing solutions. These cements are better able to form apatite (bioactivity) and are more reactive than conventional calcium silicate cements. The improved bioactivity can be attributed to the formation of F-substituted apatites, which have a K_{sp} lower than hydroxy-carbonate apatite. F-doped calcium silicate cements are promising materials for use in contact with bone in endodontics and oral surgery.

References

Abdullah D, Ford TR, Papaioannou S, Nicholson J, McDonald F (2002) An evaluation of accelerated Portland cement as a restorative material. *Biomaterials* **23**, 4001–10.

Amberg CH, Luk HC, Wagstaff KP (1974) The fluoridation of nonstoichiornetric calcium hydroxyapatite. An infrared study. *Canadian Journal of Chemistry* **52**, 4001–6.

Bhadang KA, Holding CA, Thissen H, McLean KM, Forsythe JS, Havnes DR (2010) Biological responses of human osteoblasts and osteoclasts to flame-sprayed coatings of hydroxyapatite and fluorapatite blends. *Acta Biomaterialia* **6**, 1575–83.

Brauer DS, Karpukhina N, Seah D, Law RV, Hill RG (2008) Fluoride-containing bioactive glasses. *Advanced Materials Research* **39-40**, 299–304.

Brauer DS, Mneimne M, Lynch E, Gillam DG, Hill RG (2010) Fluorapatite-forming bioactive glasses for use in dentifrices treating dentine hypersensitivity. *Journal of Dental Research* **89A**, 3758.

BSI, British Standards Institution (2007) Terminology for the bio-nano interface. *PAS (Publicly Available Specification)* **132**, 2.

Cartmell S (2009) Controlled release scaffolds for bone tissue engineering. *Journal of Pharmacological Sciences* **98**, 430–41.

Colin A, Prati C, Pelliccioni GA, Gandolfi MG (2010) Solubility in water or DMEM of F-doped MTA cements with increasing F-content. *Dental Materials* **26S**, e67.

Gandolfi MG, Farascioni S, Pashley DH, Gasparotto G, Prati C (2008a) Calcium silicate coating derived from Portland cement as treatment for hypersensitive dentine. *Journal of Dentistry* **36**, 565–78.

Gandolfi MG, Perut F, Ciapetti G, Mongiorgi R, Prati C (2008b) New Portland cement-based materials for endodontics mixed with articaine solution: a study of cellular response. *Journal of Endodontics* **34**, 39–44.

Gandolfi MG, Ciapetti G, Perut F *et al.* (2009a) Biomimetic calcium-silicate cements aged in simulated body solutions. Osteoblasts response and analyses of apatite coating. *Journal of Applied Biomaterials & Biomechanics* **7**, 160–70.

Gandolfi MG, Iacono F, Agee K *et al.* (2009b) Setting time and expansion in different soaking media of experimental accelerated calcium-silicate cements and ProRoot MTA. *Oral Surgery, Oral Medicine, Oral Pathology, Oral Radiology & Endodontics* **108**, e39–45.

Gandolfi MG, Taddei P, Tinti A, Dorigo De Stefano E, Rossi PL, Prati C (2010a) Kinetics of apatite formation on a calcium-silicate cement for root-end filling during ageing in physiological-like phosphate solutions. *Clinical Oral Investigations* **14**, 659–68.

Gandolfi MG, Van Landuyt K, Taddei P, Modena E, Van Meerbeek B, Prati C (2010b) ESEM-EDX and raman techniques to study MTA calcium-silicate cements in wet conditions and in real-time. *Journal of Endodontics* **36**, 851–7.

Gandolfi MG, Taddei P, Tinti A, Prati C (2010c) Apatite-forming ability of ProRoot MTA. *International Endodontic Journal* **43**, 917–29.

Gandolfi MG, Ciapetti G, Taddei P *et al.* (2010d) Effect of ageing on bioactivity and in vitro biological properties of calcium silicate-cements for dentistry. *Dental Materials* **26**, 974–92.

Gandolfi MG, Prati C (2010e) MTA and F-doped MTA cements used as sealers with warm gutta-percha. Long-term sealing ability study. *International Endodontic Journal* **43**, 889–901.

Holden DT, Schwartz SA, Kirkpatrick TC, Schindler WG (2008) Clinical outcomes of artificial root-end barriers with mineral trioxide aggregate in teeth with immature apices. *Journal of Endodontics* **34**, 812–7.

Kokubo T, Takadama H (2006) How useful is SBF in predicting in vivo bone bioactivity? *Biomaterials* **27**, 2907–15.

Lau KHW, Baylink DJ (1998) Molecular mechanism of action of fluoride on bone cells. *Journal of Bone and Mineral Research* **13**, 1660–7.

Lin Q, Li Y, Lan X, Lu C, Chen Y, Xu Z (2009) The apatite formation ability of CaF_2 doping tricalcium silicates in simulated body fluid. *Journal of Biomedical Materials Research* **4**, 1–6.

Maeno S, Niki Y, Matsumoto H *et al.* (2005) The effect of calcium ion concentration on osteoblast viability, proliferation and differentiation in monolayer and 3D culture. *Biomaterials* **26**, 4847–55.

Nair PNR (2006) On the causes of persistent apical peridontitis: a review. *International Endodontic Journal* **39**, 249–81.

Nair PNR, Duncan HF, Pitt Ford TR, Luder HU (2008) Histological, ultrastructural and quantitative investigations on the response of healthy human pulps to experimental capping with mineral trioxide aggregate: a randomized controlled trial. *International Endodontic Journal* **41**, 128–50.

Nakade O, Koyama H, Arai J, Ariji H, Takada J, Kaku T (1999) Stimulation by low concentrations of fluoride of the proliferation and alkaline phosphatase activity of human dental pulp cells in vitro. *Archives of Oral Biology* **44**, 89–92.

Pace R, Giuliani V, Pagavino G (2008) Mineral trioxide aggregate as repair material for furcal perforation: case series. *Journal of Endodontics* **34**, 1130–3.

Parirokh M, Torabinejad M (2010) Mineral trioxide aggregate: a comprehensive literature review – Part III: clinical applications, drawbacks, and mechanism of action. *Journal of Endodontics* **36**, 400–13.

Qu H, Wei M (2006) The effect of fluoride contents in fluoridated hydroxyapatite on osteoblast behaviour. *Acta Biomaterialia* **2**, 113–9.

Qu WJ, Zhong DB, Wu PF, Wang JF, Han B (2008) Sodium fluoride modulates caprine osteoblast proliferation and differentiation. *Journal of Bone and Mineral Metabolism* **26**, 328–34.

Saunders WP (2008) A prospective clinical study of periradicular surgery using mineral trioxide aggregate as a root-end filling. *Journal of Endodontics* **34**, 660–5.

Sun J, Wei L, Liu X *et al.* (2009a) Influence of ionic dissolution products of dicalcium silicate coating on osteoblastic proliferation, differentiation and gene expression. *Acta Biomaterialia* **5**, 1284–93.

Sun J, Li J, Liu X, Wei L, Wang G, Meng F (2009b) Proliferation and gene expression of osteoblasts cultured in DMEM containing the ionic products of dicalcium silicate coating. *Biomedicine & Pharmacotherapy* **63**, 650–7.

Sundfeldt M, Persson J, Swanpalmer J *et al.* (2002) Does sodium fluoride in bone cement affect implant fixation Part II: evaluation of the effect of sodium fluoride additions to acrylic bone cement and the fixation of titanium implants in ovariectomized rabbits. *Journal of Materials Science: Materials in Medicine* **13**, 1045–50.

Taddei P, Tinti A, Gandolfi MG, Rossi PL, Prati C (2009a) Vibrational study on the bioactivity of portland cement-based materials for endodontic use. *Journal of Molecular Structure* **924-926**, 548–54.

Taddei P, Tinti A, Gandolfi MG, Rossi PL, Prati C (2009b) Ageing of calcium silicate cements for endodontic use in simulated body fluids: a micro-Raman study. *Journal of Raman Spectroscopy* **40**, 1858–66.

Taddei P, Modena E, Tinti A, Siboni F, Prati C, Gandolfi MG (2011) Vibrational investigation on the in vitro bioactivity of commercial and experimental calcium-silicate cements for root-end endodontic therapy. *Journal of Molecular Structure* **993**, 367–75.

Torrisi A, Torrisi V, Tuccitto N, Gandolfi MG, Prati C, Licciardello A (2010) Tof SIMS images and spectra of biomimetic calcium-silicate based cements after storage in solutions simulated the human biological fluid effects. *International Journal of Mass Spectrometry* **289**, 150–61.

Tuna D, Ölmez A (2008) Clinical long-term evaluation of MTA as a direct pulp capping material in primary teeth. *International Endodontic Journal* **41**, 273–8.

Xu Z, Lin Q, Li Y, lan X, Lu C (2008) An evaluation of CaF2 doping tricalcium silicate as dental restorative materials. *Advanced Materials Research* **47-50**, 1339–42.

Yoon BH, Kim HW, Lee SH, Bae CJ, Koh YH (2005) Stability and cellular responses to fluorapatite–collagen composites. *Biomaterials* **26**, 2957–63.

Zhang WG, Wang LZ, Liu Z (1998) The influence of fluoride on the development of the osteoblast phenotype in rat calvarial osteoblasts: an in vitro study. *Shanghai Kou Qiang Yi Xue* **7**, 88–93.